



Prediction of the tidal turbine power fluctuations from the knowledge of incoming flow structures

Philippe Druault ^{a,*}, Grégory Germain ^b

^a Sorbonne Université, CNRS, Institut Jean Le Rond d'Alembert, F-75005 Paris, France

^b IFREMER, Marine Structure Laboratory, 150 quai Gambetta, 62200 Boulogne-sur-mer, France

ARTICLE INFO

Keywords:

Turbine power fluctuations
Large scale flow structures
Stochastic estimation
Proper orthogonal decomposition
Fourier analysis

ABSTRACT

After positioning a 1:20 scaled model of a three-bladed horizontal-axis turbine in the wake of a wall-mounted cylinder, synchronized turbine performance and flow measurements are carried out to investigate the relationship between the incoming flow field and the turbine power fluctuations. The Linear Stochastic Estimation (LSE) is used to predict the turbine output fluctuations from the knowledge of the Large Scale flow Structures (LSS) embedded in the incoming turbulent flow. LSS extraction by Fourier analysis or Proper Orthogonal Decomposition shows that LSS are responsible for the main unsteady variations of the power fluctuations, especially their highest amplitudes. The RMS of turbine output fluctuations are entirely due to the LSS. It is also demonstrated that whatever the nature of the incoming turbulent flow is, the low frequency filtering process coupled with the LSE method allows the recovering of at least 90% of the turbine power RMS. Furthermore, the low-frequency spectral content of the turbine power fluctuations is very well predicted, especially the frequency peaks. A preliminary LSE application is performed in order to predict the instantaneous turbine output fluctuations at more than 85% confidence level, from only three velocity signals measured in front of the turbine.

1. Introduction

To improve the energy extraction efficiency from tidal turbines and also the prediction of energy production, it becomes essential to better assess the effect of environmental flow conditions on the turbine response output. Indeed, to limit the uncertainty in energy predictions, one has to identify how the nature of the incoming flow affects not only the turbine power generation, but also the blade structural fatigue and the operational life. Furthermore, the development of mathematical tools to predict the energy power fluctuations is important to future control the turbine parameters and then to reduce the fluctuating electrical power feed into the grid.

The effect of flow perturbations, due to small and large scale flow structures (length scales) and to different turbulence intensity, has already been reported and studied (Blackmore et al., 2016; Ouro and Stoesser, 2019; Gaurier et al., 2020a; Allmark et al., 2020; Thiébaut et al., 2020). Tidal turbines in a farm can be also submitted to wake effect, constituting an additional source of instability (Ebdon et al., 2020; Slama et al., 2021). Even if marine currents are more predictable, tidal turbines meet the same problem as wind turbine but it is accentuated by the proximity of the free surface and the seabed, both of which present high variability due to the wave and bathymetry variations (Adcock et al., 2020).

Previous studies (Durán Medina et al., 2017; Gaurier et al., 2020a; Gao et al., 2020) show that, when regarding the turbine output response under turbulent flow conditions, the turbine power and thrust signals are well correlated to inflow conditions. Thus, the link between organized large scale flow structures and turbine outputs has been assessed through statistical analyses based on temporal correlations (Gaurier et al., 2020b). Temporal correlation analyses between incoming turbulence and blade structural responses also shown that blade structural response varies as a function of the flow length-scales (Gao et al., 2020). Recent work has also shown how the large dominant turbulent scales of incoming flow affect the spectral characteristics of turbine power, i.e., determining the level and trend of the turbine power spectrum (Ahmadi and Yang, 2021). From all those studies, it is now well admitted that in the spectral domain the turbine power exhibit three main contributions: (i) a low-frequency large-scale flow structure signatures, (ii) frequency peaks associated with the turbine rotor frequency (f_r) and with the blade passing frequency ($3 \times f_r$) (iii) the small-scale background turbulence signature which leads to a $-11/3$ power decay in the high frequency domain (Druault et al., 2022).

* Corresponding author.

E-mail addresses: philippe.druault@sorbonne-universite.fr (P. Druault), gregory.germain@ifremer.fr (G. Germain).

As recently outlined by Adcock et al. (2020), the characterization of the unsteady turbulent flow loading of turbine blades and its prediction remain a key problem. Even if the origin of the turbine power variability is generally due to the large scale flow structures present in turbulent flows, understanding the relationship between incoming flow variations and turbine power ones is required. Moreover, even if some methods exist to calculate the power production fluctuations especially in wind industry (Pinson and Madsen, 2012; Lu et al., 2021), the development of new mathematical post-processing tools for predicting the instantaneous turbine power fluctuations is of interest to improve the turbine operation, especially for predicting the blade structural fatigue of the turbine.

The purpose of this study is to reconstruct (and to predict) the turbine output fluctuations from the knowledge of the incoming velocity and to quantify how the dynamic of large-scale dominant flow structures present in high Reynolds number turbulent flow are responsible for the turbine power fluctuations. To this aim, we study how Large Scale flow Structures (LSS) generated in the wake of a wall-mounted cylinder (Ikhenicheu et al., 2019a) impact the behavior of a 1 : 20 scaled model of a three-bladed horizontal-axis turbine. Synchronous measurements of the incoming velocity field and turbine thrust and torque are carried out at different turbine locations in the wake of the cylinder in order to establish the link between the velocity fluctuations and the turbine behavior. From these results, we will propose a process to reconstruct both turbine thrust and power signals with the aim of quantifying the effect of LSS onto (i) the instantaneous turbine output fluctuations, (ii) the Root Mean Square of these fluctuations and (iii) the spectral content of the turbine output fluctuations.

After detailing the experimental set-up, mathematical post-processing tools implemented in this work are described in Section 3. These tools rely on a judicious coupling between Linear Stochastic Estimation and Fourier analysis or Proper Orthogonal Decomposition. Both of these last methods are used to extract the large scale flow structure embedded in the turbulent flow. Then the turbine thrust and power signals are reconstructed from the knowledge of the large scale flow structures and the linkage between both quantities are discussed in Section 4. The last part is devoted to the reconstruction of turbine output fluctuations from a very limited number of velocity signals allowing a new way for the control of the fluctuations of the energy generation process.

2. Experimental database

In this section we briefly recall the experimental set-up as well as the available measurements. These have been extensively detailed in several previous papers (Ikhenicheu et al., 2019b; Gaurier et al., 2020a,b; Druault et al., 2022).

In the wave and current circulating flume tank of IFREMER with a test section of 18 m long × 4 m wide × 2 m deep, an uniform steady incoming flow ($U_\infty, V_\infty, W_\infty$) is generated with a low turbulence intensity of $I_\infty = 1.5\%$. This incoming flow interacts with a wall bottom-mounted cylinder which is considered to reproduce a specific bathymetry. The height of the square wall-mounted cylinder is of $H = 0.25$ m and its length is of $6H$. It is scaled to real sea conditions of a tidal site (Ikhenicheu et al., 2019b). The Froude similitude is respected with $F = U_\infty/(gD) = 0.23$ with g the gravity and D the tank depth. In the wake of this cylinder, a single 1/20 scaled tri-bladed horizontal axis tidal turbine is successively positioned at four streamwise locations: $x^* = x/H = [4; 10; 16; 23]$ (Fig. 1). The instrumented scale turbine has a diameter $D = 2R = 0.72$ m and is positioned at mid-depth in the tank. In each test case, the nominal Tip Speed Ratio at $TSR = \omega R/U_\infty = 4$, with ω the rotational frequency, is imposed (Magnier et al., 2020).

For each of the four turbine positions a same experiment is conducted where the velocity field and the turbine thrust and power are measured simultaneously. Thrust T and rotor torque Q experienced by the rotor are measured by a torque and thrust transducer without

friction effect (the instrumentation is located upstream of the shaft seal) (Gaurier et al., 2015; Druault et al., 2022). Recall that the turbine power is determined as follows: $P = \omega Q$. Instantaneous velocity vector fields in a vertical plane in front of the turbine are obtained thanks to Particle Image Velocimetry (PIV) (Fig. 1) measurements. The three instantaneous velocity components are denoted (U, V, W) along the (x, y, z) directions respectively. Only one vertical PIV measurement plane located just in front of the operating turbine is considered. For each location, the plane is centered vertically at the hub height and ends horizontally at the blade root. It is discretized on 330×840 pixels², corresponding to a physical meshgrid of $(N_x \times N_z) = (30 \times 74)$ with a spatial discretization of 11.2 mm. Velocity and Thrust-Torque measurements are synchronized with a same time duration, $T = 180$ s with a sampling frequency of $f_{PIV} = 15$ Hz and $f_T = 120$ Hz respectively. Such time duration ($N_t = 2700$ instants) corresponds to 40 large eddy turnover times, assuring the statistical convergence of the data (Ikhenicheu et al., 2019b).

Due to shadowing effect in the measurement plane, the instantaneous velocity field extracted along a vertical line (N_z points) at the x-centered plane position is only retained for the next analyses.

In this paper, the following fluctuating variables are used: u' , T' and P' corresponding to the streamwise velocity component, the turbine thrust and the turbine power respectively. These fluctuating variables are directly deduced from the classical Reynolds decomposition.

3. Mathematical post-processing: Stochastic estimation coupled with FFT or POD filtering methods

After recalling the theoretical linkage between fluctuating velocity field and the turbine variables, the Linear Stochastic Estimation (LSE) is presented. Then, the LSE method is coupled with Fourier or Proper Orthogonal Decomposition (POD) demonstrating how the turbine thrust and power can be reconstructed from the knowledge of large scale coherent structures.

3.1. Relationship between turbine thrust-power and inflow velocity fluctuations

Following previous developments (Bossuyt et al., 2017; Bandi, 2017; Druault et al., 2022), the instantaneous turbine performance-related parameters based on the disk average reference velocity field are linearly dependent on the instantaneous velocity field. More precisely, assuming that the inflow velocity fields is available in a grid mesh of N points, sweeping the rotor area, the instantaneous fluctuating performance-related parameters can be expressed as follows (after neglecting high order terms Bossuyt et al., 2017; Druault et al., 2022):

$$T'(t) \simeq K_1 \sum_{i=1}^N u'(t, i) \text{ and } P'(t) \simeq K_2 \sum_{i=1}^N u'(t, i) \quad (1)$$

where (K_1, K_2) are two real constants depending of (C_T, \bar{U}^2) and (C_P, \bar{U}^3) respectively. C_P and C_T are the power and thrust coefficients respectively, which are supposed to be constant, and \bar{U} is the mean streamwise velocity component over the rotor area. Note that only the streamwise velocity component is retained as it usually dominates the other velocity components.

As a linear relationship exists between performance-related parameters and incoming fluctuating velocity fields, the purpose of the following analysis is then to propose a method allowing the reconstruction of these turbine parameters thanks only to the knowledge of the fluctuating velocity field at few selected locations.

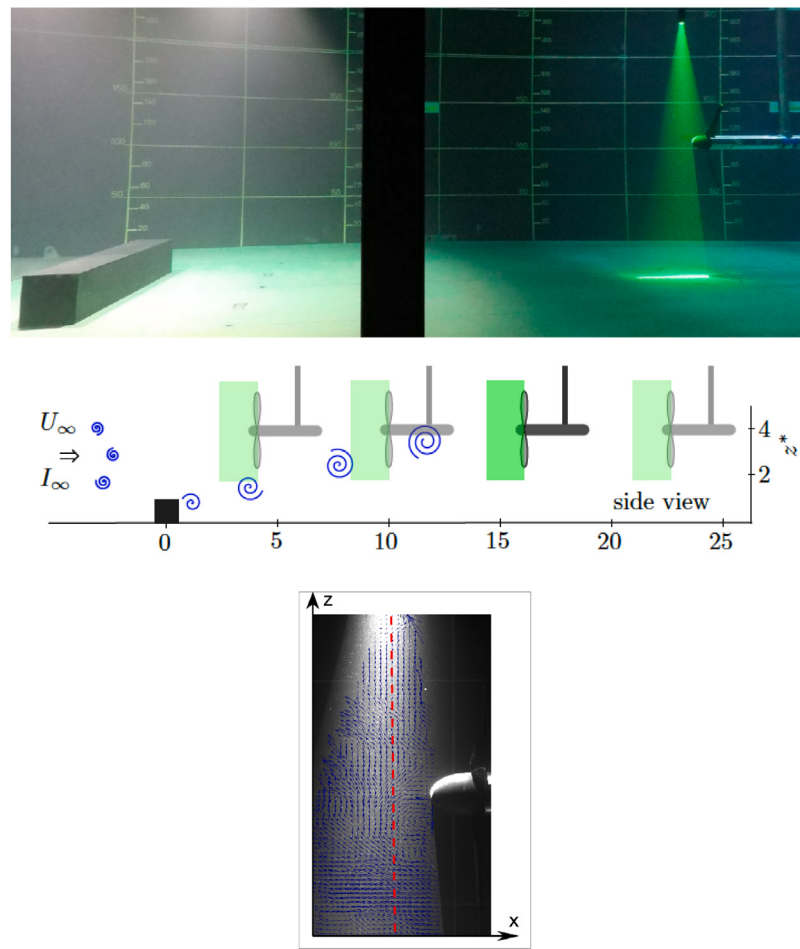


Fig. 1. Top: Experimental set-up including the wall-mounted cylinder, the horizontal-axis turbine model and the PIV laser sheet in front of the rotor (this picture corresponds to the turbine position $x^* = 16$). Middle: Turbine and PIV vertical measurement plane locations. Bottom: Illustration of an instantaneous velocity vector measurement and the location of the vertical line under consideration.

3.2. Linear Stochastic Estimation (LSE)

Mathematically, the Stochastic Estimation (SE) method provides an approximation (or estimation) of a random variable in terms of some other random variables which are known. Historically, the application of stochastic estimation to turbulent flow relies on a reconstruction of the conditional average of the field based on the knowledge of several measurements signals (Adrian and Moin, 1988). Briefly, the estimation uses a specified conditional event about the flow at one or more locations together with its statistical properties to estimate the information at surrounding locations, allowing the reconstruction of the large scale flow structures embedded in a turbulent flow (Adrian and Moin, 1988; Druault et al., 2005; Murray and Ukeiley, 2007). Previous applications proposed to estimate a flow variable from the knowledge of the same flow variable. However, SE can also be used to estimate a flow variable from a conditional event which is associated with another flow variable (Picard and Delville, 2000; Druault et al., 2010; Durgesh and Naughton, 2010; Druault et al., 2011).

In the present work, as fluctuating performance-related parameters are linearly dependent on the fluctuating velocity field, stochastic estimation can be used to reconstruct these parameters from the knowledge of the velocity field. The mathematical development is detailed below for the turbine power reconstruction. A similar procedure for the turbine thrust reconstruction can be followed.

Assuming that velocity measurements are available at N_z points, Eq. (1) leads to:

$$P'_{rec}(t) = \sum_{i_z=1}^{N_z} A(i_z) u'(t, i_z) \quad (2)$$

The time-independent coefficient A is determined by minimizing the quadratic error $\langle |P'_{rec} - P'|^2 \rangle$. This yields the following system of equations:

$$\overline{u'(i_z) u'(i_z)} A(i_z) = \overline{u'(i_z) P'} \quad (3)$$

An overbar indicates the time average operation. This system can be symbolically written in the matrix form, $R_{uu} A = R_{uP}$, where R_{uP} is the matrix of the velocity-turbine power correlation between $u'(i_z, t)$ and $P'(t)$ respectively and R_{uu} is the matrix of auto-correlations. As this last matrix is invertible, matrix coefficient A is thus solution of the matrix system:

$$A = R_{uu}^{-1} R_{uP} \quad (4)$$

The LSE implementation requires the knowledge of the covariance matrix between the conditional events (here the fluctuating velocity field measured at selected reference points) as well as the covariance matrix between the conditional events and the turbine power, the variable to estimate.

3.3. Coherent structure extraction: Fourier or POD analysis

As an objective is to reconstruct the turbine performance parameters due to the large scale flow structures, one has to first consider a triple decomposition of the instantaneous velocity field, $u(z, t)$: the time averaged part ($\bar{u}(z)$) and the fluctuating contribution ($u'(z, t)$) which is decomposed into a coherent part and an incoherent part:

$$u(z, t) = \bar{u}(z) + u'(z, t) = \bar{u} + \tilde{u}(z, t) + u''(z, t) \quad (5)$$

The coherent part \tilde{u} corresponds to the coherent flow structures (denoted LSS for Large Scale flow Structures) and the incoherent one u'' is related to Background Turbulence (BT). There are multiple approaches for separating the large scale organized flow structures and its background turbulent counterpart. In the present study, to isolate the flow structures, two methods are implemented: the Fourier analysis denoted FFT (Fast Fourier Transform) and the Proper Orthogonal Decomposition (POD).

When dealing with FFT method, the aim of the decomposition is to extract the periodic contributions associated with LSS. In this context, the Large Scale flow Structures are parametrized by the frequency domain under interest and filtered thanks to FFT application. As turbulent flow structures are of low frequency content, then a low-pass filter in frequency domain is applied. The frequency cut-off is denoted f_c . At each z location, the filtered fluctuating velocity field is then obtained by following these steps: (i) compute the FFT of the fluctuating velocity field, (ii) put to zero value the FFT result for frequencies higher than f_c and (iii) perform an inverse Fourier Transform to recover the filtered velocity field, denoted \tilde{u}_{FFT} . To control the abruptness of the low-pass window, an exponential-law decreasing is used without noticeable differences on the filtered results presented below, compared to a Heaviside low-pass filter.

In the other hand, the purpose of POD application is to isolate the energetic flow structures. POD is a mathematical post-processing tool leading to a linear decomposition of the velocity field. As this POD technique is based on an optimal energetic decomposition, the first POD modes are associated with these energetic flow structures. This contribution will be denoted \tilde{u}_{POD} . Briefly, the POD method which is a powerful method of data analysis, has been introduced in turbulence by Lumley (1967) to extract the large scale energetic flow structures from turbulent flows. It consists in finding among a set of realizations of the flow field, the realization which maximizes the mean square energy that leads to resolve the Fredholm integral eigenvalue problem

$$\int_S R_{uu}(z, z') \phi^{(n)}(z', t) dz' = \lambda^{(n)} \phi^{(n)}(z, t), \quad (6)$$

where $R_{uu}(z, z')$ is the time averaged two-point spatial correlation tensor, S is the spatial domain and z denotes the spatial coordinate. $\phi^{(n)}$ corresponds to the n th eigenfunction (or mode) of the correlation tensor and $\lambda^{(n)}$ is the associated eigenvalue and corresponds to the turbulent kinetic energy contained in mode number n , if all the velocity components are considered. The eigenfunctions of this correlation tensor are mutually orthogonal by construction and they are usually chosen to be orthonormal:

$$\int_S \phi^{(n)}(z) \phi^{(m)}(z) dz = \delta_{nm}, \quad (7)$$

with δ the Kronecker symbol. The projection of the velocity field (fluctuating random function) onto $\phi^{(n)}$ gives the projection coefficients, $b^{(n)}(t)$, which are uncorrelated: $b^{(n)}(t) b^{(m)}(t) = \delta_{nm} \lambda^{(n)}$. The velocity component u' can be then exactly represented by a linear combination of deterministic mutually orthonormal modes weighted by these random coefficients:

$$u'(z, t) = \sum_{n=1}^{N_{mod}} b^{(n)}(t) \phi^{(n)}(z), \quad (8)$$

where N_{mod} is the number of the total POD mode number. It corresponds to the rank of the kernel, the correlation tensor. In the present study, the classic POD is considered: $N_{mod} = N_z$ as $N_t > N_z$.

Using Eq. (8), the extraction of the LSS contribution is done by truncated the first N_m modes and the background incoherent turbulence by the POD mode remainder

$$\tilde{u}_{POD}(z, t) = \sum_{n=1}^{N_m} b^{(n)}(t) \phi^{(n)}(z) \text{ and } u''_{POD}(z, t) = \sum_{n=N_m+1}^{N_{mod}} b^{(n)}(t) \phi^{(n)}(z) \quad (9)$$

The choice of N_m separating background turbulence to coherent flow structures is still a debate in the turbulence community. In the following, the selection of N_m will be done from an energetic criterion.

3.4. Complementary technique: LSE coupled with Fourier or POD method

The purpose of the complementary technique is to extract the large-scale flow contribution from the turbulent flow and to use it as conditional event to reconstruct the variable to estimate. The LSE/POD complementary technique has been already applied to estimate and predict the behavior of energetic flow structures (Bonnet et al., 1994; Durgesh and Naughton, 2010; Druault et al., 2011). Based on previous developments (Eqs. (2) and (5)), the instantaneous turbine power fluctuations conditioned by the Large Scale flow Structures are then estimated as follows:

$$\tilde{P}(t) = \sum_{i_z=1}^{N_z} A(i_z) \tilde{u}_{method}(z, t) \text{ with method=FFT or POD} \quad (10)$$

and the turbine power associated with Background Turbulence (BT):

$$P''(t) = \sum_{i_z=1}^{N_z} A(i_z) u''_{method}(z, t) \text{ with method=FFT or POD} \quad (11)$$

By comparing with the power signals measured experimentally, it will be possible to quantify the flow field contribution which governs the main power variations.

3.5. Remarks

First, in previous sub-sections, the common LSE approach is derived where a zero time lag is considered between both quantities: velocity field and turbine power. To improve the reconstruction of the turbine power, the time-delay must be taken into account (Durgesh and Naughton, 2010). Consequently, before calculating the spatial correlation between u' and P' , the optimal time-lag (τ) between both quantities must be estimated. The time-independent coefficient A will be then determined from the spatial correlation R_{uP} computed from $u'(i_z, t + \tau)$ and $P'(t)$ and the resulted LSE equation becomes:

$$P'_{rec}(t) = \sum_{i_z=1}^{N_z} A(i_z) u'(t + \tau, i_z) \quad (12)$$

When reconstructing the turbine power from only the Large Scale flow Structures (Eq. (10)), the computation of the spatial correlation R_{uP} can be done from two possibilities: either from reference velocity field $u'(i_z, t + \tau)$ and $P'(t)$ or from Large Scale flow Structures velocity field $\tilde{u}_{method}(i_z, t + \tau)$ and $P'(t)$. In the following, the matrix A is always determined from the spatial correlation R_{uP} computed from the reference velocity field $u'(i_z, t + \tau)$ and $P'(t)$. This solution is more adapted for a future turbine control strategy. Indeed, one of the most attractive features of the stochastic estimation is that the majority of the data processing is performed only once, independently of the conditions being investigated.

4. Analysis of synchronous velocity and thrust-torque measurements

First the incoming turbulent wake-cylinder flow is analyzed with an emphasis of the Large Scale flow Structure characterization. Second, the turbine output measurements are commented as a function of the turbine location in the cylinder wake. Then, preliminary statistical analyses between incoming flow and turbine-performance parameters are presented.

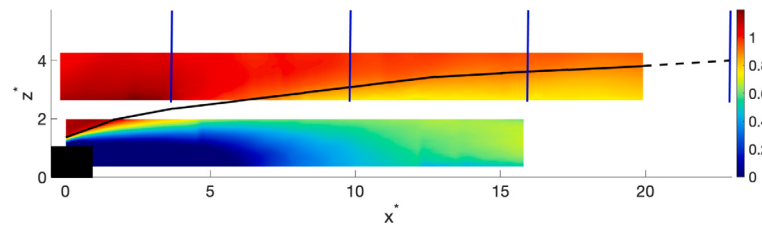


Fig. 2. Mean streamwise velocity component in the symmetrical $y = 0$ plane. Black line indicates the location where $\bar{U} = 0.9U_\infty$. Purple lines indicate the locations of the turbine: $x^* = 4, 10, 16$ and 23 . (For interpretation of the references to color in this figure legend, the reader is referred to the web version of this article.)

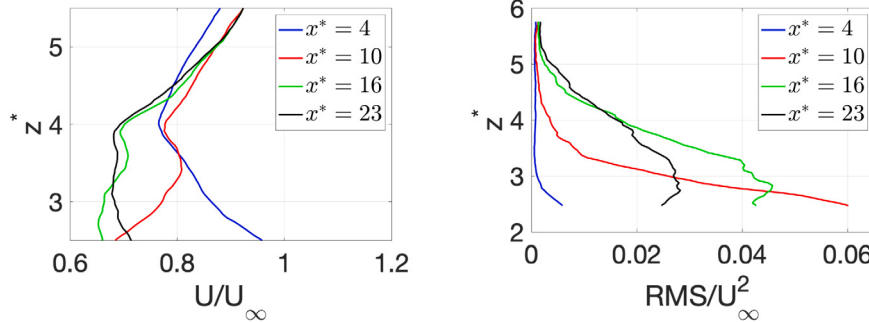


Fig. 3. Mean streamwise velocity component (left hand side) and associated Root Mean Square (right hand side) along the z vertical direction in front of the turbine for the 4 configurations: $x^* = 4, 10, 16$ and 23 . (For interpretation of the references to color in this figure legend, the reader is referred to the web version of this article.)

4.1. Characterization of the incoming velocity field

Fig. 2 displays the mean streamwise velocity component obtained from previous PIV measurements (Ikhenicheu et al., 2019a; Druault et al., 2022). This picture shows the horizontal and vertical spatial development of the cylinder wake. Purple lines indicate the 4 turbine locations ($x^* = x/H = [4; 10; 16; 23]$) in the experiments detailed above. The black line shows the position of the $\bar{U} = 0.9U_\infty$ border. It is then observed that the first turbine position ($x^* = 4$) is located in a uniform flow field with a slight flow acceleration area at the bottom of the turbine. Conversely, the three other turbine positions, $x^* = [10; 16; 23]$ are in the cylinder wake flow where a vertical shear velocity profile is present. Fig. 3 presents the mean streamwise velocity component and its associated Root Mean Square (RMS) $\sqrt{u'^2}$, along the vertical line in front of each turbine location. The induction mechanism is clearly highlighted. The shear velocity profiles are noticeably modified by the presence of the turbine at its nominal functioning point. The blockage effect due to the hub is also clearly visible, especially at $x^* = 4$ when the incoming flow is quasi uniform along the vertical direction, in absence of the turbine. The most important shear flow modifications are observed in the lower part of the turbine ($z^* < 4$) due to the presence of different velocity shear profiles along the x direction (Fig. 2). The turbulence activity, u'^2 is also mainly concentrated in this lower part as the flow is more uniform in the upper part of the turbine (Fig. 3-right).

The velocity spectral content is presented in Fig. 4. The velocity signal is extracted at three selected locations: $(z_1^*, z_2^*, z_3^*) = (3, 4, 5)$ for each of the four configurations. The spectral content differs as a function of the streamwise positions. The amplitude of the velocity spectra in the $x^* = 4$ section is quite smaller than the one in the other streamwise sections, especially in the lower part of the rotor swept area, (z_1^*, z_2^*) . Furthermore, at $x^* = 4$, the velocity field does not exhibit any frequency peak whatever the z location is, as the flow is mainly uniform in this area and no large scale flow structures emerge. Far downstream, the frequency signature of the large scale energetic flow structures is clearly indicated in the lower part of the rotor swept area while at z_3^* the frequency peak is less pronounced. This confirms previous analyses in similar flow configurations (Ikhenicheu et al., 2019a; Druault et al., 2022) where low-frequency large-scale structures

are rising in the far wake. An interesting feature is the small frequency peak observed around $f = 5.4\text{Hz}$ corresponding to the blade passing frequency ($3 \times f_r$).

To extract periodic flow structures a low pass filter can be applied in the spectral domain by canceling spectral for frequencies higher than f_c . In the following, $f_c = 1\text{ Hz}$ is chosen. This value is retained because it is at least twice smaller than the integral time-scales which are superior to 2 Hz in each streamwise section (Druault et al., 2022).

Moreover, to extract energetic dominant large scale flow structures from PIV measurements, the POD is used to decompose instantaneous streamwise velocity fluctuating component available along vertical z -line for each available velocity database: $u'(z, t) = \sum_{n=1}^{N_{mod}} b^{(n)}(t)\phi^{(n)}(z)$ with $N_{mod} = 74$. Fig. 5 represents the energy distribution $\sum_{n=1}^N \lambda^{(n)} / \sum_{i=1}^{N_{mod}} \lambda^{(i)}$ as well as the cumulative sum $\lambda^{(N)} / \sum_{i=1}^{N_{mod}}$, computed in each of the four velocity database. As expected, the POD energy content of the velocity field measured in front of the turbine located at $x^* = 4$ is seen to be very distributed over a wide range of POD modes. This confirms that no energetic flow structures emerge in this section as the flow is mainly uniform with a low energy content (see Fig. 3). In the three other streamwise sections, the first POD mode contains more than 60% of the total energy emphasizing that large scale energetic structures are present. Thus, in sections $x^* = 10$ and $x^* = 16$, 8 POD modes represent more than 90% of the total energy while in section $x^* = 23$, 11 POD modes are necessary to recover at least 90%. This last result shows that far upstream, the wake flow is less organized with more background turbulence.

An illustration of the extraction of the large scale structures is provided in Fig. 6, for the streamwise location, at $x^* = 16$. The instantaneous fluctuating reference streamwise velocity component is projected onto the first 8 POD modes corresponding to 90% of the total energy (N_{m90}):

$$\tilde{u}_{POD}(z, t) = \sum_{n=1}^{N_{m90}} b^{(n)}(t)\phi^{(n)}(z) \quad (13)$$

The same reference velocity field filtered with FFT analysis using $f_c = 1\text{ Hz}$ is also represented for comparison. To better understand where the small discrepancies arise, the difference of both filtered velocity fields relative to the reference case is also represented in Fig. 6. The

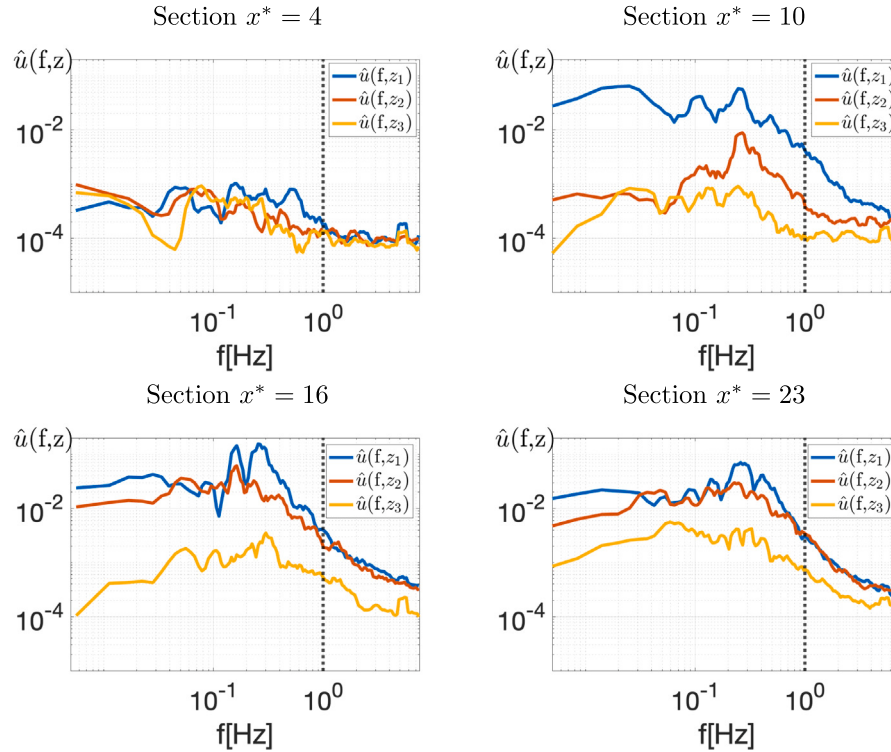


Fig. 4. Velocity spectra $\hat{u}(f, z_i^*)$ with $z_1^* = 3$, $z_2^* = 4$ and $z_3^* = 5$ computed in front of the turbine for the 4 configurations. Vertical dotted-line indicates the cut-off frequency choices: $f_c = 1$ Hz. (For interpretation of the references to color in this figure legend, the reader is referred to the web version of this article.)

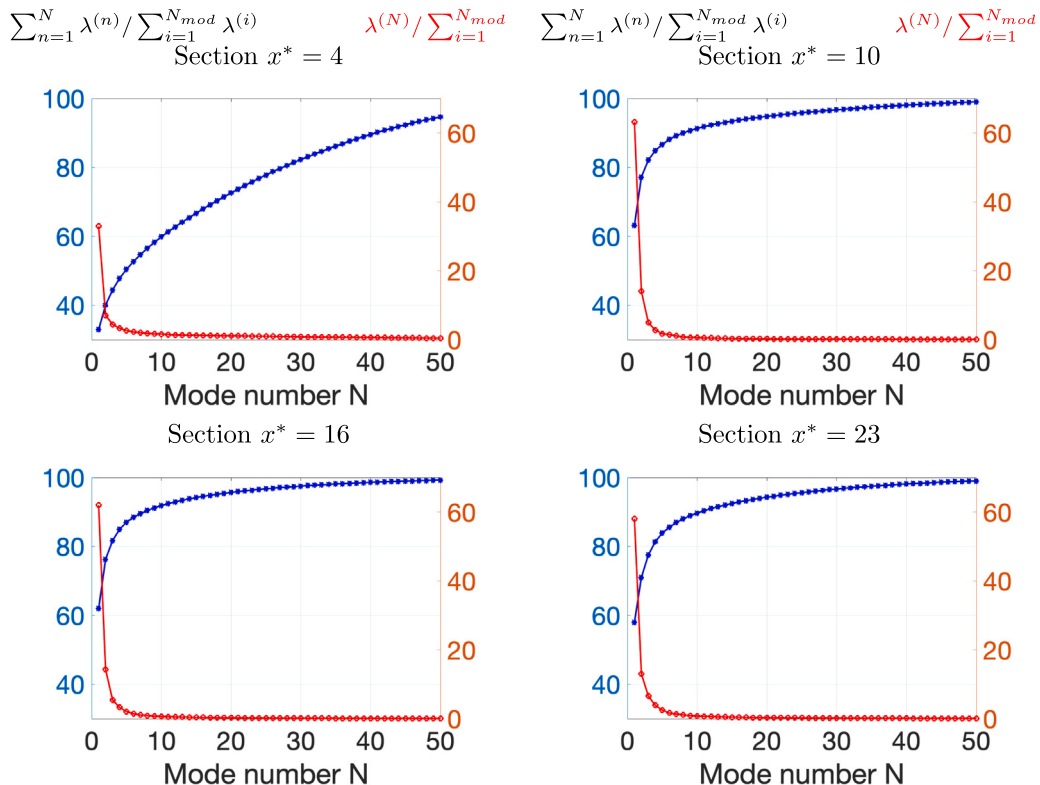


Fig. 5. POD energy distribution and the cumulative sum of the first 50 modes out of the $N_z = 74$ modes for the 4 test configurations: $x^* = 4$ (Top-left), $x^* = 10$ (Top-right), $x^* = 16$ (bottom-left), $x^* = 23$ (bottom-right). (For interpretation of the references to color in this figure legend, the reader is referred to the web version of this article.)

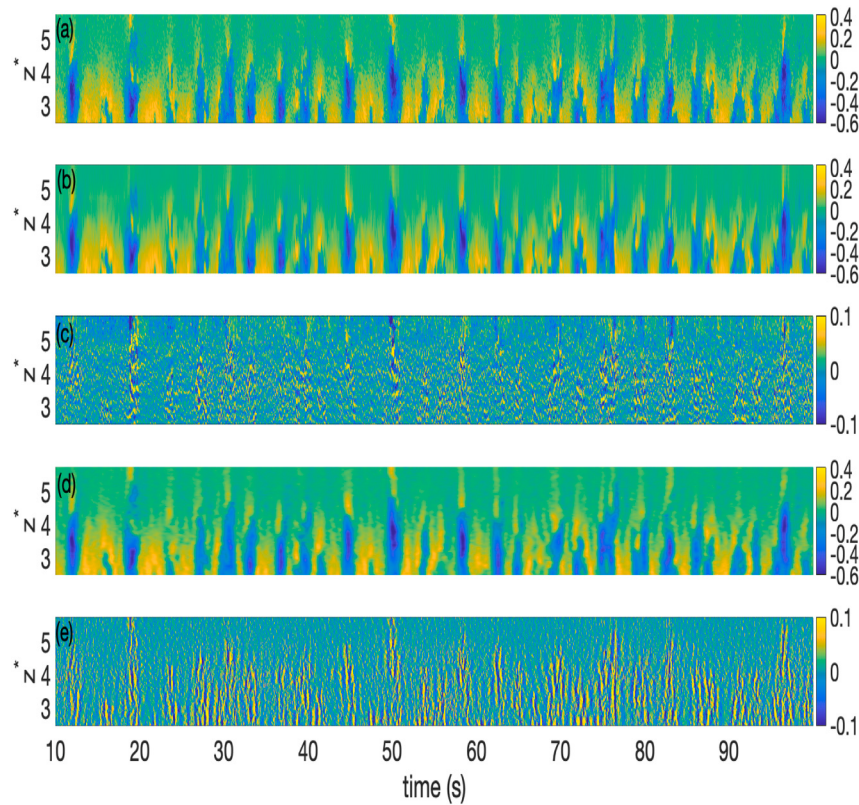


Fig. 6. $x^* = 16$ location. Top to bottom: (a) reference fluctuating streamwise velocity component, (b) and (c) projection onto the first N_{m90} POD modes and its difference from the reference velocity field, (d) and (e) FFT filtered velocity field using $f_c = 1$ Hz and its difference from the reference velocity field. X -axis is limited to 100 s to better observe the differences. (For interpretation of the references to color in this figure legend, the reader is referred to the web version of this article.)

dominant flow structures identified with the vertical sign change in the fluctuating streamwise velocity component, are clearly extracted from each method, mainly in the lower part of the z domain, $z^* < 4$.

The energetic content of the reconstructed velocity fields is provided in Fig. 7 (right). Whatever the z -locations a similar energy deficit is observed for $\bar{u}_{POD}(z, t)$ using N_{m90} .

The associated spectral content is displayed in Fig. 7 (left). The spectra of \bar{u}_{FFT} is exactly similar to the reference one until the cut-off frequency (not represented). Similarly, the spectra of \bar{u}_{POD} is in a very good agreement with the reference one in the low frequency domain, especially in presence of LSS ($z = z_1$). It is interesting to observe that the low frequency peaks of \bar{u}_{POD} are more pronounced than the ones of reference data and blade passage frequency peak ($f = 5.4$ Hz) is also more present compared to the reference velocity field. The low energetic content for $z^* > 4.5$ is confirmed even if the low frequency peak is more pronounced.

4.2. Turbine thrust and power measurements

The mean turbine-performance parameters (thrust and power) are indicated in Table 1. The thrust and power mean values are directly linked to the mean streamwise velocity values (Bossuyt et al., 2017; Bandi, 2017; Druault et al., 2022). Indeed, the maximum values are obtained when the turbine is positioned in section $x^* = 4$ when the mean values are around 20% higher than those in the far wake streamwise sections where the speed of the flow is reduced leading to smaller turbine-performance parameters mean values. The highest values of turbine thrust and power variations are observed in the far wake positions ($x^* = 16$ and $x^* = 22$) where the turbulent velocity intensity increases (see Fig. 3). This confirms that high levels of incoming turbulence intensity lead to an increase of the turbine-performance variations (Ebdon et al., 2020). These preliminary measurements emphasize that

Table 1
Mean and root mean square, σ_T of the turbine thrust and power.

x^*	\bar{T} (N)	σ_T (N)	σ_T/\bar{T}	\bar{P} (W)	σ_P (W)	σ_P/\bar{P}
4	211.7	4.3	0.02	105.86	4.42	0.04
10	194.1	9.5	0.05	89.60	8.05	0.09
16	178.0	19.1	0.11	77.20	13.05	0.17
23	174.1	18.8	0.11	73.45	13.48	0.18

the nature of the flow impacting a single turbine can greatly modifies the turbine power fluctuations. Thus, by just modifying the turbine position in the wall-mounted cylinder wake, the mean and RMS turbine performances vary notably from 4% to 18%.

Fig. 11 represents the thrust spectra (black line) for each flow configuration. When comparing these spectra to those of incoming velocity field (Fig. 4) similar characteristics are seen for frequencies $f < 1$ Hz. Above these frequencies, the frequency peak associated with the blade frequency passage $3 \times f_p = 5.4$ Hz is well exhibited in the thrust spectra like in previous works (Chamorro et al., 2015). In the inertial frequency range, the spectra follows a power law decay of $-11/3$, as discussed previously (Druault et al., 2022).

4.3. Temporal correlation between incoming velocity and turbine performance

To study the coupling between turbine-parameters and incoming turbulent flow, a direct temporal-correlation between instantaneous fluctuating streamwise velocity component $u'(z, t)$ and instantaneous turbine thrust force $T'(t)$ (or turbine power $P'(t)$) is computed:

$$R_{uT}(z, \tau) = \frac{\overline{u'(z, t)T'(t + \tau)}}{\sigma(u')\sigma(T')} \quad \text{and} \quad R_{uP}(z, \tau) = \frac{\overline{u'(z, t)P'(t + \tau)}}{\sigma(u')\sigma(P')} \quad (14)$$

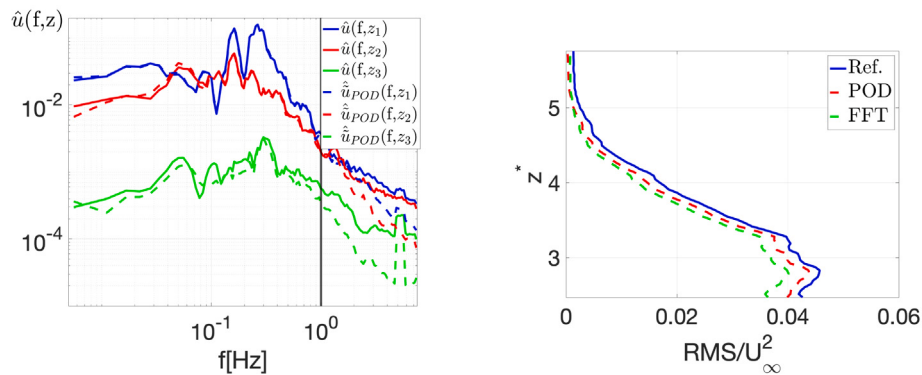


Fig. 7. Left: Reference velocity spectra $\hat{u}(f, z^*)$ with $z_1^* = 3$, $z_2^* = 4$ and $z_3^* = 5$ computed at $x^* = 16$ superimposed onto spectra computed from $\tilde{u}_{POD}(z, t)$ using N_{m00} . Vertical dotted-line indicates the cut-off frequency, $f_c = 1$ Hz. Right: Root Mean Square along the z vertical direction at $x^* = 16$ superimposed onto the RMS computed from $\tilde{u}_{POD}(z, t)$ using $N_m = 8$ and from $\tilde{u}_{FFT}(z, t)$ using $f_c = 1$ Hz. (For interpretation of the references to color in this figure legend, the reader is referred to the web version of this article.)

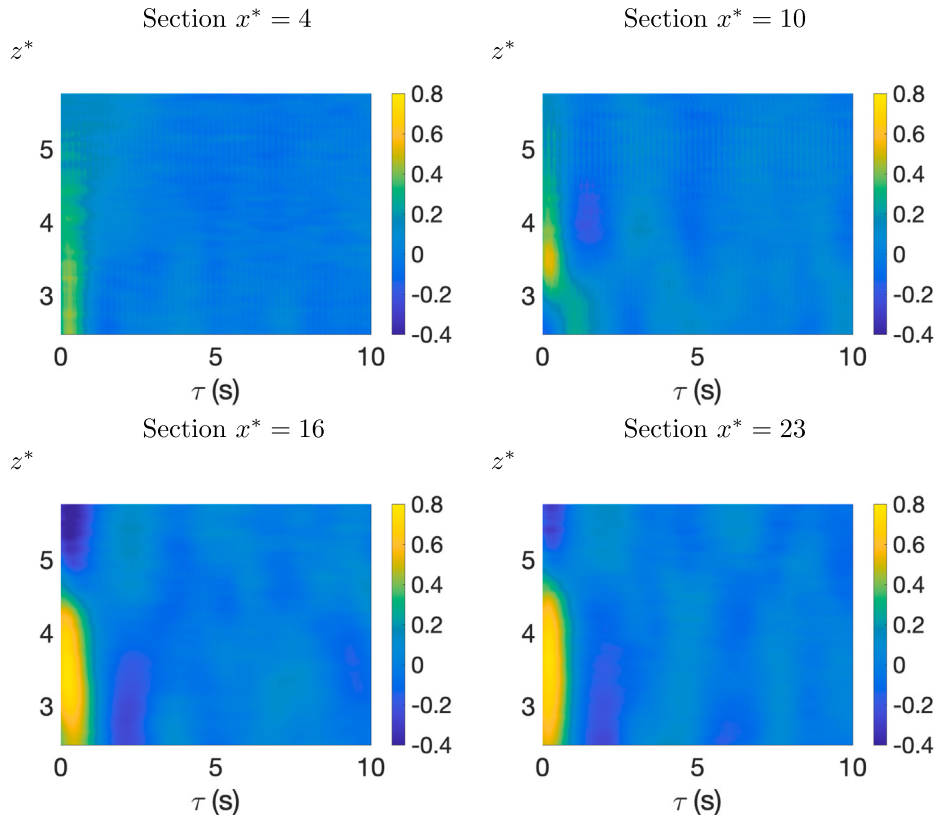


Fig. 8. Time delay (τ s) x-axis of the normalized correlation of the incoming streamwise velocity component with the turbine thrust, for the 4 configurations. (For interpretation of the references to color in this figure legend, the reader is referred to the web version of this article.)

where τ is the time lag and σ the RMS value. Fig. 8 shows the resulted $R_{uT}(z, \tau)$ for the four configurations. Quasi-similar results (not shown) are obtained for $R_{uP}(z, \tau)$.

Higher levels of temporal correlation are observed for $z^* < 4$ that corresponds to the area where large scale flow structures impact the turbine. At $x^* = 4$, no clear correlations between PIV measurements and turbine thrust are present. It is directly related to the low energetic uniform flow in this streamwise section. The other temporal correlation isosurfaces ($x^* \geq 10$) show that large scale flow structures detected along the vertical line are of 2D nature and are very well correlated to the turbine performance parameters, even if only vertical line-measurements are available.

In each flow configuration, the maximum temporal correlation is obtained for $\tau = 0.27$ s, corresponding to the flow convection effect.

5. Stochastic estimation of turbine performance fluctuations

Based on previous developments, LSE is implemented to reconstruct the turbine-performance parameters for each of the four experimental configurations. First, instantaneous raw PIV velocity field measured at $N_z = 74$ positions are used as conditional events to reconstruct the turbine parameters. Second, the turbine thrust and power are reconstructed using as conditional event, the Large Scale flow Structures (LSS) extracted thanks to FFT or POD method. At last, three comparative analyses are successively done to investigate the reconstructed parameters: instantaneous, energetic and spectral analyses.

5.1. LSE reconstruction from instantaneous raw PIV database

In each flow configuration, the following procedure is done:

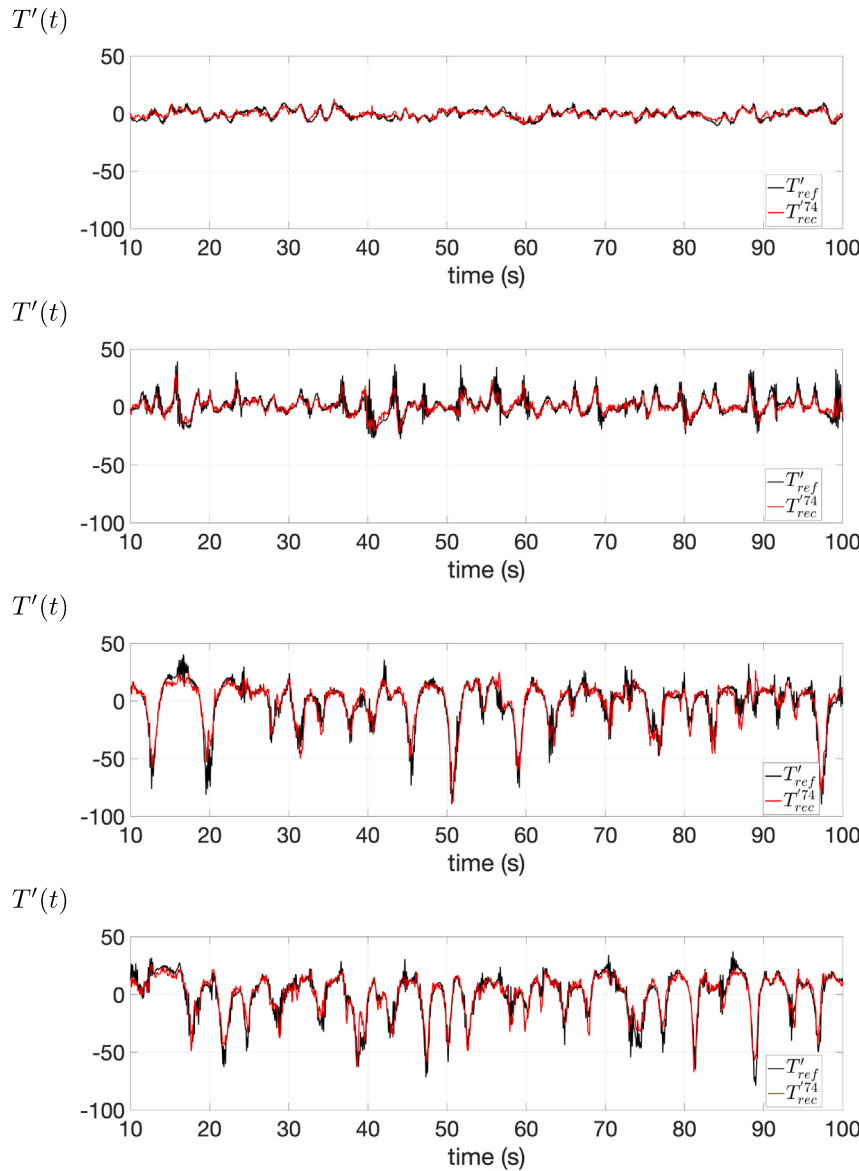


Fig. 9. Time evolution of the instantaneous LSE reconstructed turbine thrust signals superimposed onto the reference power and thrust measurements (black line) for the 4 configurations: from top to bottom: $x^* = 4, 10, 16$ and 23 . X-axis is voluntary limited to [10 : 100] s. (For interpretation of the references to color in this figure legend, the reader is referred to the web version of this article.)

1. Temporal correlation between simultaneous PIV velocity field and turbine measurements are first estimated by considering the optimal time delay, $\tau = 0.27$ s (convection effect),
2. Calculation of the time-independent temporal coefficients (Eq. (4)),
3. Reconstruction of the fluctuating turbine thrust and power by using available instantaneous PIV streamwise velocity components at the $N_z = 74$ points, taking into account the convection effect (Eq. (12)).

Figs. 9 and 10 represent the instantaneous turbine thrust and power temporal signals reconstructed for each turbine location. These signals are superimposed onto the associated reference measured signals. First, these plots reveal the effect of the flow nature on the performance of the turbine. As stated previously (see Table 1), the variabilities of turbine thrust and power generation increase as the flow variations increase. The Large Scale Structure passage is clearly indicated thanks to a great increase of the turbine thrust and power fluctuations. Based on these graphs, it is observed that LSE reconstructed signals are quite very well

correlated to the reference signal even if only 74 instantaneous velocity fields along a vertical line are used as conditional event. This result remains true whatever the level of the flow variations. Indeed, the small instantaneous variations due to the low flow energy content at $x^* = 4$ as well as the highly ones due to the large scale flow structure passage are very well reproduced thanks to the LSE reconstruction procedure. This emphasizes that the turbulent flow in front of the rotor area, impacting the turbine is very correlated to the PIV turbulent field measurements along the vertical centered line only (here positioned at $0.2H$ in front of the rotor).

The correlations calculated between the measured turbine thrust signal and the LSE reconstructed one are the following ones: 0.81, 0.78, 0.91, 0.92 for the turbine location $x^* = 4, 10, 16$ and 23 respectively. This correlation is higher at the two last locations due to the presence of 2D organized large scale flow structures that have been very well captured by PIV measurements.

Note that turbine thrust and power have a very similar temporal correlation with incoming streamwise velocity component (see Section 4.3) and also a similar expression (see Eq. (1)). Only results from

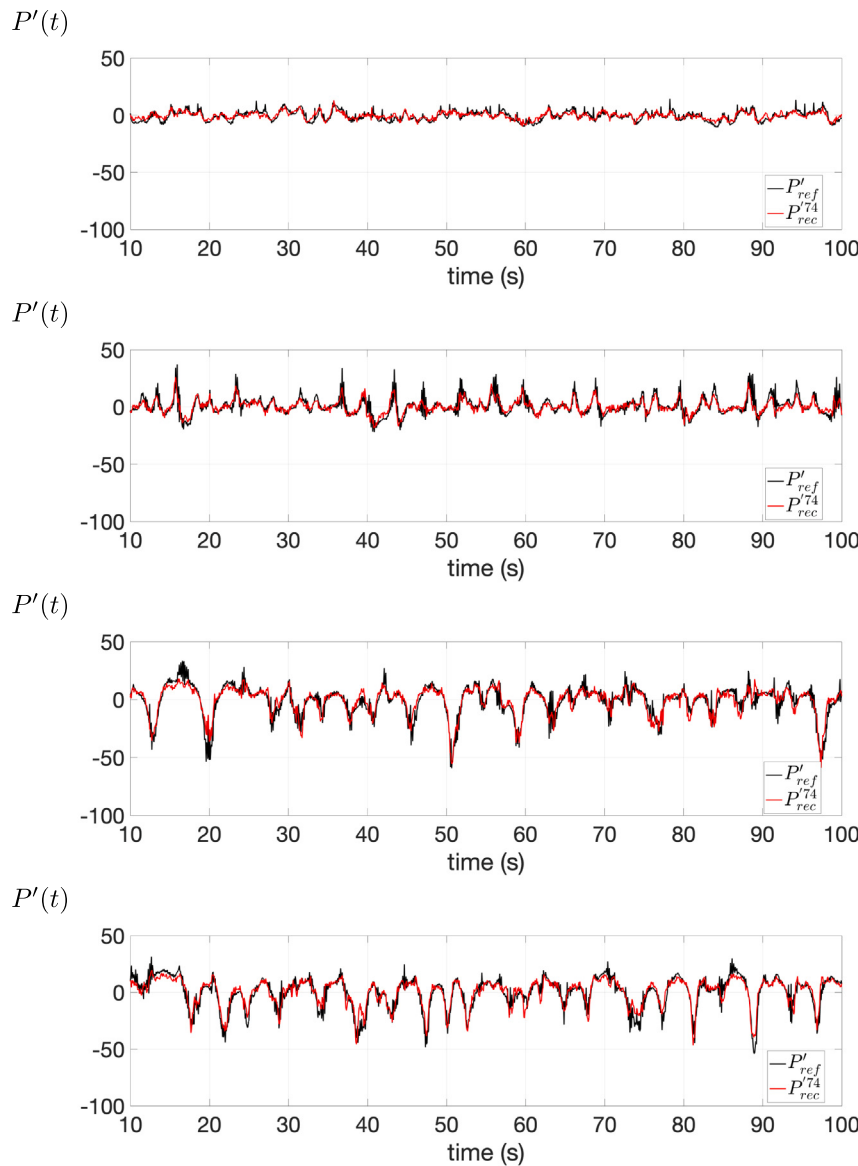


Fig. 10. Time evolution of the instantaneous LSE reconstructed turbine power signals superimposed onto the reference power and thrust measurements (black line) for the 4 configurations: from top to bottom: $x^* = 4, 10, 16$ and 23 . X -axis is voluntary limited to [10 : 100] s.

reconstructed thrust are then presented in the following and similar conclusions are obtained for the power generation fluctuations.

The spectral content of the LSE reconstructed force signals, \hat{T}_{rec} , from a FFT analysis is presented in Fig. 11 (red lines). The low frequency content of the thrust spectra is very well predicted in the reconstructed signals, especially when this low frequency content is directly linked to the Large Scale flow Structures (at $x^* = 16$ and $x^* = 23$). The frequency peak arising from the blade passage ($f = 5.4$ Hz) is not marked in the reconstructed signal as it was very poorly marked in velocity spectra (see Fig. 4).

Table 2 indicates the root mean square ratio between reconstructed signals and reference ones, $\sigma_{\hat{T}_{rec}} / \sigma_{T_{ref}}$. At sections $x^* = 4$ and $x^* = 10$, around 80% of the RMS is recovered while upstream (at $x^* = 16$ and $x^* = 23$) more than 90% is recovered. These differences are directly related to the nature of the flow where more 2D organized flow structures are present in the far cylinder wake.

Previous analyses demonstrate that from selected velocity measurements points (here $N_z = 74$), Linear Stochastic Estimation allows the reconstruction of the turbine thrust and power signals having

Table 2

RMS ratio $\sigma_{\hat{T}_{rec}} / \sigma_{T_{ref}}$ of the reconstructed the turbine thrust, by considering the entire velocity signals (top line) LSS: Large Scale flow Structures, BT: Background Turbulence. f_c is the cut-off frequency separating both LSS and BT contributions. N_m is the POD mode number separating both LSS and BT contributions and the indicated percentage corresponds to the energy content.

Filter		$x^* = 4$	$x^* = 10$	$x^* = 16$	$x^* = 22$
No	$\sigma_{\hat{T}_{rec}} / \sigma_{T_{ref}}$	0.80	0.79	0.91	0.92
FFT: $f < f_c = 1$ Hz LSS	$\sigma_{\hat{T}_{rec}} / \sigma_{T_{ref}}$	0.73	0.73	0.89	0.90
FFT: $f > f_c = 1$ Hz BT	$\sigma_{T'_{rec}} / \sigma_{T_{ref}}$	0.32	0.28	0.20	0.21
POD: $N < N_m = 8$ (90%) LSS	$\sigma_{\hat{T}_{rec}} / \sigma_{T_{ref}}$	0.80	0.77	0.91	0.92
POD: $N > N_m = 8$ (10%) BT	$\sigma_{T'_{rec}} / \sigma_{T_{ref}}$	0.06	0.16	0.10	0.08

very similar properties with the reference measured ones, not only from a statistical point of view (RMS and spectral content) but also instantaneously. These preliminary results allow then the analysis of the contribution of the flow that mainly contributes to the turbine performance fluctuations.

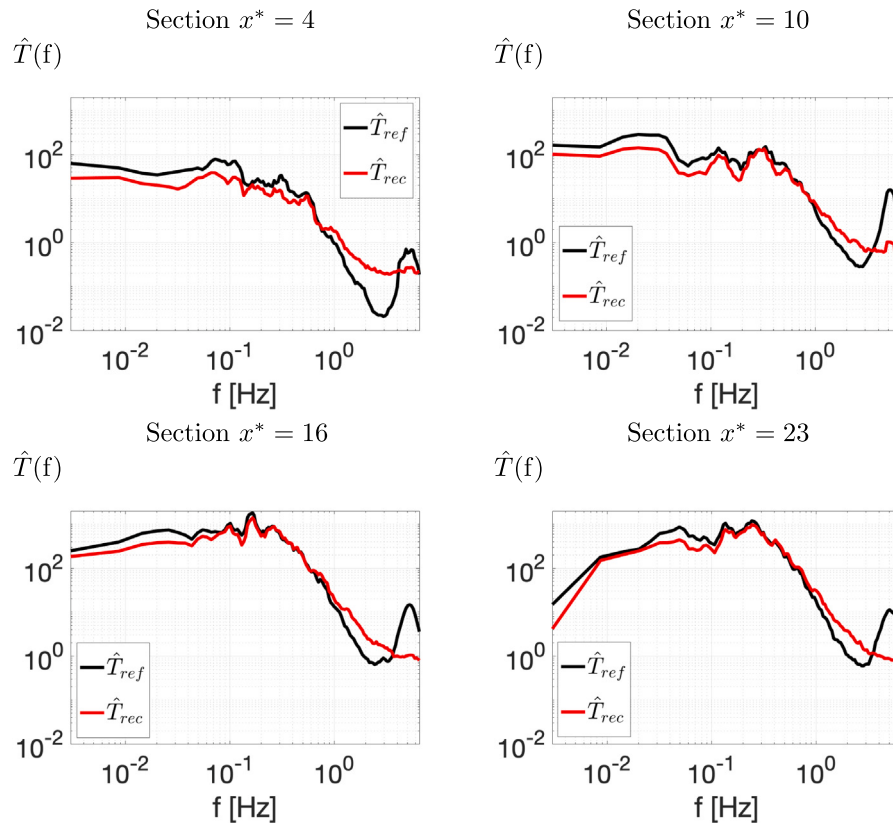


Fig. 11. Spectra of the LSE reconstructed turbine thrust (red line) superimposed on the reference thrust spectra (black line), for the 4 configurations. (For interpretation of the references to color in this figure legend, the reader is referred to the web version of this article.)

5.2. Reconstruction of the turbine performance from filtered velocity field

As detailed above, instantaneous streamwise velocity field is filtered in the spectral domain using the cut-off frequency $f_c = 1$ Hz. The low frequency filtered part of the flow field, $\tilde{u}_{FFT}(z, t)$ corresponds to the low-frequency periodical LSS. In a similar way, energetic LSS are extracted thanks to POD application using $N_m = 8$ ($N_m = 11$ at $x^* = 23$) representing 90% of the kinetic energy. Then, Linear Stochastic Estimation is now implemented to reconstruct the turbine performance parameters from the knowledge of Large Scale flow Structures (LSS) extracted from FFT or POD, $\tilde{u}_{FFT}(z, t)$ or $\tilde{u}_{POD}(z, t)$. The associated incoherent counterpart (denoted BT-Background Turbulence, u'') of the turbulent flow field is also used as conditional event to reconstruct these parameters. By comparing these results to those presented in the previous section taking into account the whole available velocity information in the LSE reconstruction process, it is then possible to quantify the effect of the filtered velocity field (LSS) on the properties of the turbine power fluctuations.

Figs. 12 and 13 display the time evolution of the reconstructed turbine thrust superimposed onto the reference one (black line), for each of the 4 turbine positions. The signals reconstructed from the LSS and BT contributions are represented by red and blue lines respectively. When LSS part is used as conditional event, the thrust signal is very well predicted, especially the highest amplitudes. Indeed, the instantaneous variations of turbine output signal are always retrieved in each case. This confirms that the highest load variations are due to the LSS events, whatever the LSS extraction method (Fourier or POD). In each case, the reconstructed thrust signal based on BT fluctuations is of very low amplitude, confirming that BT does not impact the most important turbine output fluctuations.

Table 2 indicates the RMS ratio of the reconstructed thrust signals. It is quite interesting to observe that in presence of LSS ($x^* = 16$

and $x^* = 23$), quasi-similar values are obtained by comparison of the reconstructed signal based on the reference non-filtered velocity field (top line in Table 2). This emphasizes that when a turbulent flow presents some persistent 2D low frequency energetic structures, they are entirely responsible of the RMS of the turbine-performance parameters. Some slightly smaller values (~0.73 versus ~0.80) are obtained for the other turbine locations ($x^* = 4$ and $x^* = 10$), where low frequency energetic flow structures are not present or less marked or do not pass through the entire rotor swept area. This demonstrates that the low frequency filtering process applied to incoming turbulent flow permits to recover 90% of the turbine power RMS. Globally, whatever the nature of the turbulent flow is (presence or not of large scale flow structures), a low frequency FFT filtering process coupled with LSE method allows the recovering of at least 90% of the turbine power RMS. When using POD as an energetic filtering, the RMS of the turbine output is always entirely found, meaning that the RMS of the turbine performance fluctuations can be entirely retrieved from the incoming POD filtered velocity field containing 90% of the kinetic energy.

The spectral content of the reconstructed thrust signals conditioned by LSS events is displayed in Fig. 14. The low frequency part of the turbine thrust fluctuation spectrum is very well reconstructed from the knowledge of the LSS, especially the frequency peaks. Whatever the LSS extraction method is (low frequency filtering or energetic filtering), it is observed that the LSS are responsible of the low frequency energetic content part of the turbine power fluctuations, especially when the turbulent flow is organized (at $x^* = 16$ and $x^* = 23$). When dealing with the FFT filtering process, as LSS counterpart is only of a low frequency content, the reconstructed thrust signal presents a roll-off values for $f > f_c$: the low frequency LSS cannot permit to recover the high frequency content of the turbine thrust fluctuation spectrum. Note that this may be not problematic in the sense that the energy content of the high frequency turbine power signal is at least 100 times smaller

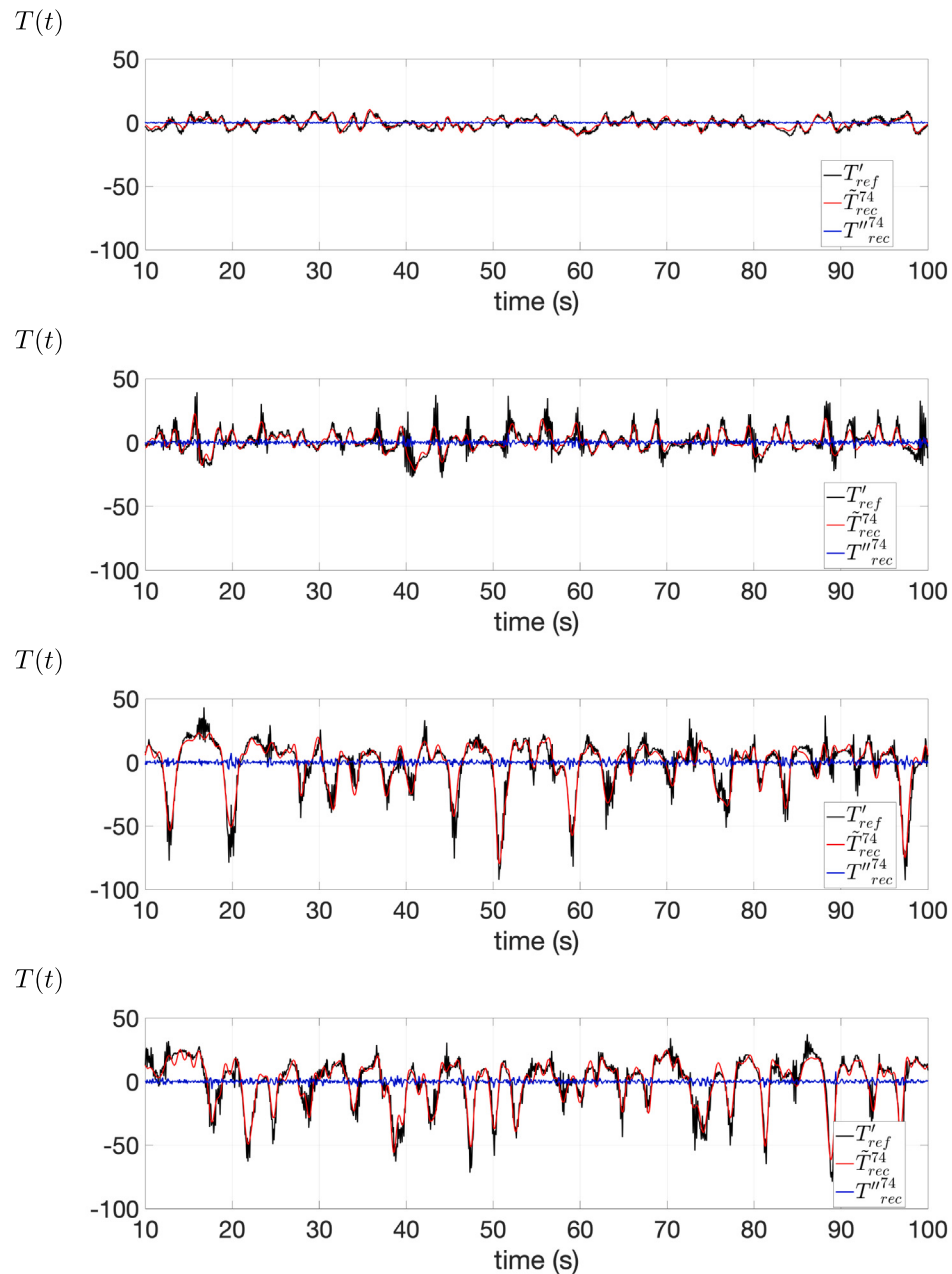


Fig. 12. Instantaneous LSE reconstructed turbine thrust signal from $\tilde{u}_{FFT}(z, t)$ using $f_c = 1$ Hz (red line) and from the background high frequency remainder (blue line), superimposed onto the reference measured thrust signal (black line), for the 4 configurations: from top to bottom: $x^* = 4, 10, 16$ and 23 . X-axis is voluntary limited to [80 : 180] s. (For interpretation of the references to color in this figure legend, the reader is referred to the web version of this article.)

than the one of the low frequency turbine power signal. In the other hand, the POD decomposition technique is a global method extracting the kinetic energy in the flow which is mainly contained in the LSS but also in smaller flow-scale structures. Consequently, when using POD to extract energetic LSS, the associated energetic LSS permits a better reconstruction of the turbine power spectrum in the whole frequency domain. If one has to focus on the high frequency behavior of the turbine thrust spectrum, POD would be preferentially best suited for the LSS filtering process. However, the effectiveness of the POD filtering application is directly related to the number of available velocity signals. Consequently in presence of a reduced number of incoming velocity signals, FFT procedure would be more appropriated.

6. Use of LSE to predict the turbine power fluctuations

As state in the introduction part, a future key challenge in the turbine operation is the real-time prediction of the turbine power fluctuations. This is of significant interest to control the turbine power fluctuations to reduce the fluctuations the generated electrical power into the grid and to limit the structural fatigue of the turbine. Even if some mathematical methods have been previously developed in wind energy (Pinson and Madsen, 2012; Lu et al., 2021), one proposes a new way for predicting the instantaneous turbine output fluctuations.

In previous sections, some mathematical tools are implemented to quantify the effect of LSS onto the turbine output fluctuations, and more specifically we demonstrate that in presence of organized LSS in a turbulent flow, LSE allows a very good estimation of the

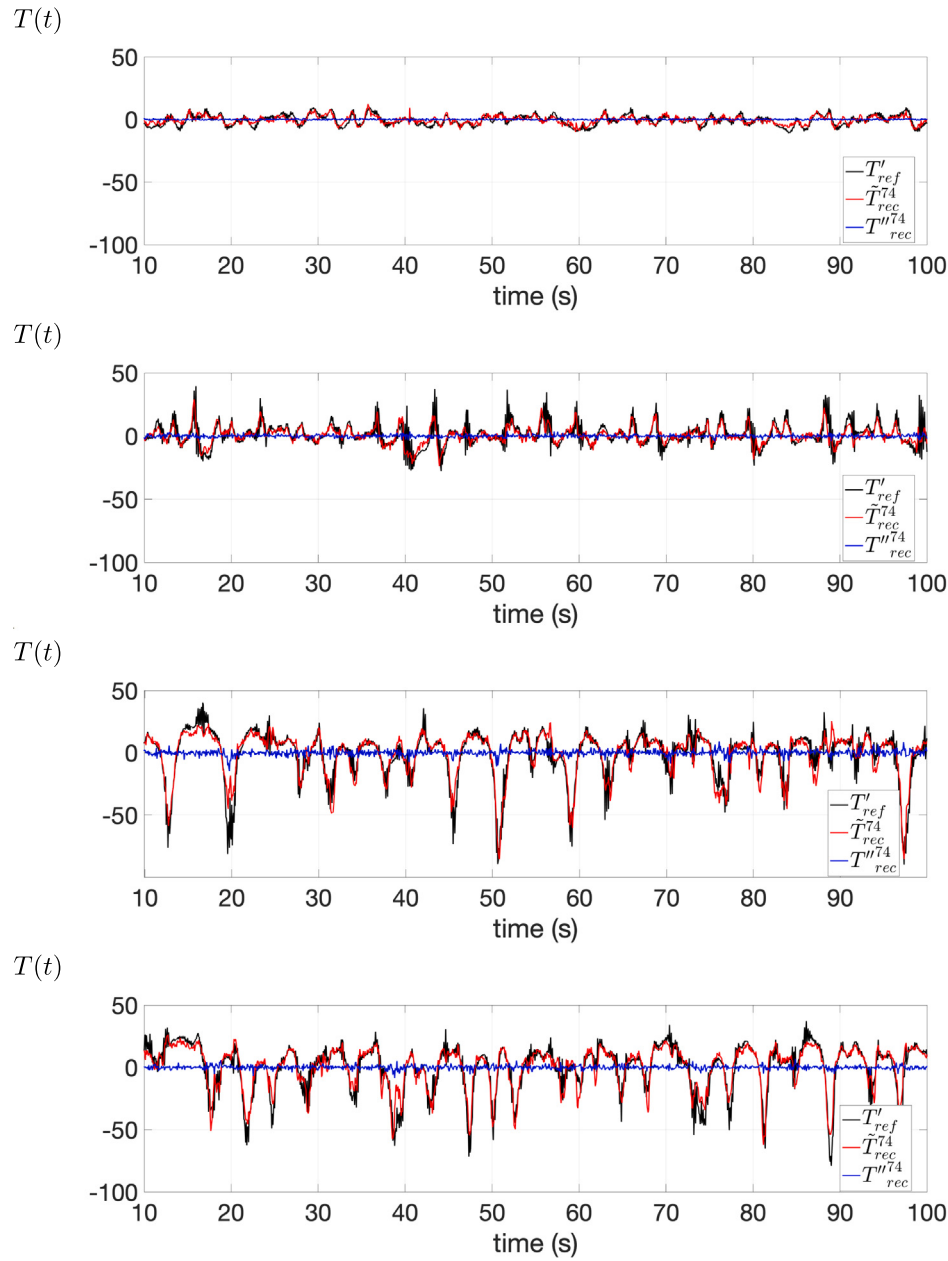


Fig. 13. Instantaneous LSE reconstructed turbine thrust force signal from $\tilde{u}_{POD}(z, t)$ using $N_m = 8$ (red line) and from the POD remainder (blue line), superimposed onto the reference thrust measurements (black line), for the 4 configurations: from top to bottom: $x^* = 4, 10, 16$ and 23 . (For interpretation of the references to color in this figure legend, the reader is referred to the web version of this article.)

unsteady turbine-performance parameters from instantaneous velocity field measured in front of the turbine (along a vertical line). In practice, the number of simultaneous measurements of incoming velocity signals in front of the turbine is very small and these velocity measurements as well as the turbine performance measurements are rarely obtained simultaneously at a sufficiently high frequency. Taken into account these remarks, as a future work, a preliminary analysis is presented in this section with the objective in showing the potential and effectiveness of the LSE to predict the turbine thrust (or power) fluctuations for the present scaled tidal turbine.

A preliminary LSE reconstruction is done by taking as conditional signal only one velocity signal.

The flow configuration for which the turbine is positioned at $x^* = 16$ is retained for this test. The following locations for the conditional velocity signals are successively retained: $z_1^* = 4.7$, $z_2^* = 3.3$ and $z_3^* = 4$, which correspond to plus and minus the mid-height of the blade and

the center of the rotor, respectively. The raw (without any filtering) streamwise velocity signal measured at each of these 3 positions is then used as conditional event for the reconstruction of the turbine thrust fluctuating signal:

$$T_{rec}^{z_i}(t) = A(z_i)u'(t + \tau, z_i) \quad \text{with } i = 1, 2 \text{ or } 3 \quad (15)$$

where the coefficient $A(z_i)$ is determined thanks to Eq. (4) based on the covariance matrix between the conditional events (here it is the fluctuating velocity field measured at only reference point) as well as the covariance matrix between the conditional events and the turbine thrust. The unsteady turbine thrust fluctuations are successively estimated from one velocity signal. Fig. 15 displays the three instantaneous estimated turbine thrust signals. The associated spectra are represented in Fig. 16. Furthermore, the RMS ratios $\sigma_{T_{rec}^{z_i}}/\sigma_{T_{ref}}$ are equal to 0.02, 0.48 and 0.47 for z_1 , z_2 and z_3 respectively. These results indicate that the reconstruction based on the velocity signal extracted at z_1 (top

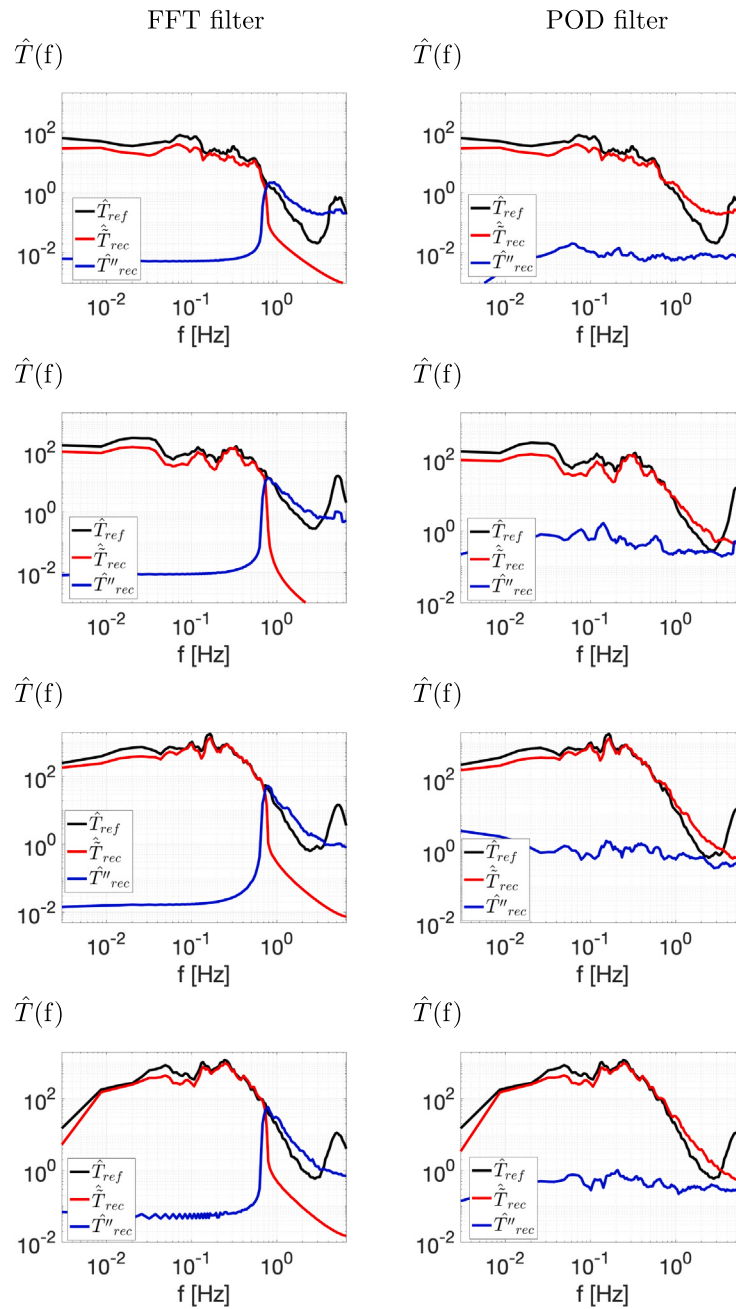


Fig. 14. Spectral representation of the turbine thrust force signal reconstructed using LSS (red line) and BT (blue line) as conditional event, superimposed on the reference measured force spectra (black line). Left column: LSS is extracted from FFT analysis using $f_c = 1$ Hz. Right column: LSS is extracted from POD method using $N_m = 8$. For the 4 configurations: top to bottom: $x^* = 4, 10, 16$ and 23 . (For interpretation of the references to color in this figure legend, the reader is referred to the web version of this article.)

mid-height of the blade) is not satisfactory. This is directly related to the poor correlation that exists between this velocity signal and the thrust signal (see Fig. 8). Conversely, when using the other velocity signal (either at z_2 or z_3) as conditional event, the reconstructed thrust fluctuations are partly recovered, with near 47% of the thrust RMS is obtained in each case. The main difference between these both last reconstructions concern the associated spectral representation of \hat{T} for which the main frequency peaks in the low frequency domain are not always well recovered. The fact that the thrust reconstructions can be quite similar or very distinct is linked to the flow coherence and its spatial extent over the turbine rotor area, as shown in Fig. 8. In presence of large scale flow structures which are very well correlated to the turbine thrust signal, one-point velocity signal containing the large scale flow passage information (spectral content as well as energetic one) can permit to reconstruct near half the thrust fluctuations content.

However, some precautions have to be taken with respect to these results because they are very flow dependent.

In this sense, to reveal the main flow dynamics of the flow sweeping the rotor-area, it is expected that one-point velocity measurement is not sufficient to establish a good linkage between incoming velocity and turbine power and to control the turbine power fluctuations, whatever the turbulent flow under consideration. In this sense and based on our experience it seems that at least 3 measurement points would be necessary to recover the main LSS dynamics of a turbulent flow which are responsible of the main turbine output fluctuations.

The flow configuration for which the turbine is positioned at $x^* = 16$ is kept for this test. The following locations for the conditional velocity signals are retained: $z_1^* = 4.7$, $z_2^* = 3.3$ and $z_3^* = 4$. The raw (without any filtering) streamwise velocity signals measured at these 3 positions

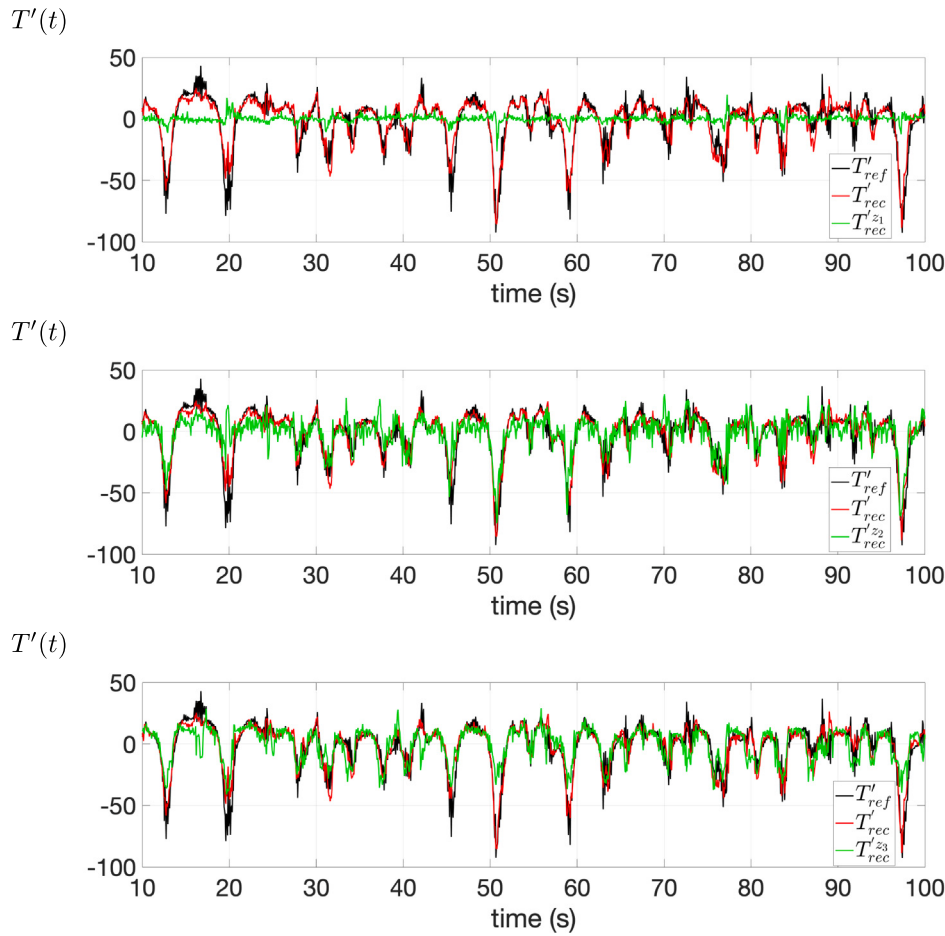


Fig. 15. Instantaneous turbine thrust signal reconstructed from one velocity signal extracted at z_i (green line) superimposed onto the reference measured one (black line) and onto the reconstructed one from all available velocity signals (N_z points). Top: z_1 , Center: z_2 , Bottom: z_3 . (For interpretation of the references to color in this figure legend, the reader is referred to the web version of this article.)

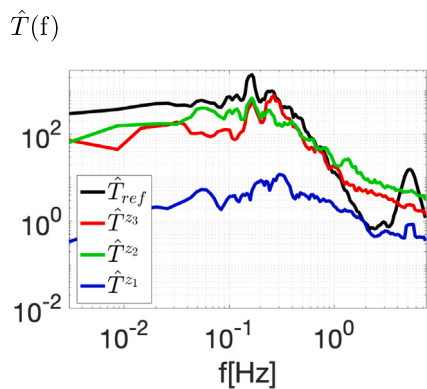


Fig. 16. Superimposition of the reconstructed thrust spectra, $\hat{T}^{z_i}(f)$ (with $z_i = z_1, z_2$, and z_3) and of the reference one $\hat{T}_{ref}(f)$. Each spectrum \hat{T}^{z_i} is computed from the reconstructed thrust signal deduced from the knowledge of one-point velocity signal extracted at the z_i location. (For interpretation of the references to color in this figure legend, the reader is referred to the web version of this article.)

are then used as conditional event for the reconstruction of the turbine thrust fluctuating signal:

$$T'_{rec}^{z_3}(t) = A(z_1, z_2, z_3)\mathbf{U}(t + \tau) \quad (16)$$

where \mathbf{U} corresponds to the three velocity signals extracted at (z_1, z_2, z_3) . Such an application allows then the prediction of the unsteady turbine thrust fluctuations from the knowledge of these three velocity signals.

Figs. 17 and 18 represent the instantaneous estimated turbine thrust signal and its associated spectrum (green line in these figures), respectively. It is observed that even with only 3 velocity signals as conditional event, the main thrust fluctuations are very well predicted as well as its spectral content. By comparison with the reconstructed thrust signal using the $N_z = 74$ available velocity measurements (red line in these figures), only a slight energy content decay is observed. The RMS ratio, $\sigma_{T_{rec}^{z_3}}/\sigma_{T_{ref}}$, is equal to 0.86 meaning that 86% of the total turbine thrust RMS is predicted with only 3 velocity signals.

These last results demonstrate that the use of only three velocity sensors in combination with the stochastic estimation and covariance statistical information allows the instantaneous prediction of the fluctuating parts of the turbine thrust and power, in a very good agreement. For in-situ conditions, if a measurement system is implemented to access to the incoming turbulent velocity field at least at three locations, a good prediction of the power generation fluctuations could be achieved. Future turbine operation strategies could then be implemented to reduce the turbine fluctuations that permits to reduce the associated fluctuations of the generated electrical power into the grid and to better limit the blade structural fatigue.

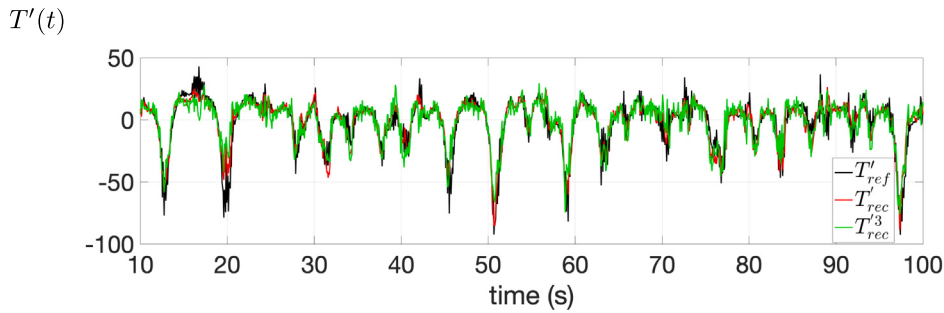


Fig. 17. Instantaneous turbine thrust signal reconstructed from the three raw velocity signals (green line) superimposed onto the reference measured one (black line) and onto the reconstructed one from all available velocity signals (N_z points). (For interpretation of the references to color in this figure legend, the reader is referred to the web version of this article.)

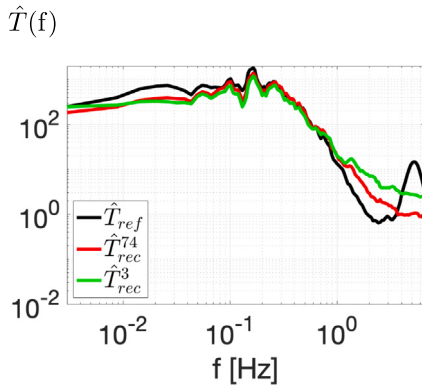


Fig. 18. Spectral representation of the thrust signal reconstructed from 3 velocity signals (green line), superimposed onto the reference case (black line) and the one reconstructed from the $N_z = 74$ available velocity measurements (red line). (For interpretation of the references to color in this figure legend, the reader is referred to the web version of this article.)

7. Conclusion

A lot of previous studies have underlined the effect of the incoming turbulent flow on the turbine power generation and the need to better understand the relationship between incoming turbulent flow and turbine performance. Previous works have also emphasized the need to develop robust mathematical methods for the prediction of the turbine power fluctuations. In this sense, by measuring simultaneously turbine-performance parameters and velocity field in front of a 1:20 scaled turbine, some mathematical tools are implemented to answer to these questions.

As turbine-performance parameters are linearly dependent of velocity field, the Linear Stochastic Estimation has been applied to predict these parameters from the measured incoming velocity fields. First, by using the whole available measured velocity signals, whatever the nature of the incoming turbulent flow, the predicted turbine-performances parameters are in very good agreement with the reference measured ones. That confirms the great relationship between both variables and the interest in using LSE method. Second, by isolating the Large Scale flow Structure contribution from the incoming turbulent flow, either from a frequency analysis (Fourier Transform) or from an energetic point of view (Proper Orthogonal Decomposition), the turbine performances are predicted using this LSS part as conditional event. It is then demonstrated that the instantaneous turbine thrust fluctuations are very well predicted from the knowledge of the LSS, especially their highest amplitudes. This result is independent of the LSS extraction method (low frequency content or energetic point of view). Even in presence of only smaller flow structures, it is demonstrated that the

low frequency filtering process applied to incoming turbulent flow is responsible of near 90% of the turbine power RMS. The low frequency part of the spectrum of the turbine thrust fluctuations is very well predicted from the knowledge of the LSS, especially the frequency peaks. Whatever the LSS extraction method, LSS are entirely responsible of the low frequency energetic content part of the turbine power fluctuations. Even if POD and FFT differ from the nature of the filtering, both filtering procedures lead to similar predicted parameters, apart in the high frequency domain where turbine-performances reconstructed from POD energetic structures are in a better agreement with reference measurements. As a matter of fact, POD is a global method based on the whole available velocity time and space information while FFT analysis extracts only localized data information, in the low frequency domain: the FFT filtering process applied individually to each measurement velocity signal always filters out the high frequency part of the signal, for frequencies superior to the cut-off frequency. When dealing with the FFT filtering, no high frequency information is available in the LSE estimation process, leading to a turbine power's response with only a signature in the low frequency domain.

Finally, a preliminary application is performed to demonstrate the potential and the effectiveness of the LSE method to predict the turbine output fluctuation from a very limited number of incoming velocity signals. By taking into account only three velocity signals (located at plus and minus the mid-height of the blade and the center of the rotor), LSE application permits to predict the RMS of the turbine-performance parameters at more than 85% confidence level, while it is not at all the case by using only one point velocity signal. Furthermore, a very good prediction of the spectrum of turbine thrust (and power) is observed.

As a future analysis, other turbulent flows have to be considered, with more three dimensional complex organization. Moreover, the effect of Tip Speed Ratio on the induced variations of the turbine-performance parameters have to be studied in the hope to future implement control strategies for reducing the amplitude of the turbine output fluctuations. Control strategies could therefore be used to adjust the optimal TSR by reducing the loading fluctuations and then limiting the fluctuations in the energy production process.

CRediT authorship contribution statement

Philippe Druault: Formal analysis, Software, Writing – original draft, Writing – review & editing. **Grégoire Germain:** Conceptualization, Methodology, Funding acquisition, Writing – review & editing.

Declaration of competing interest

The authors declare that they have no known competing financial interests or personal relationships that could have appeared to influence the work reported in this paper.

Acknowledgments

This research was partly funded by the European Commission H2020 Programme for Research & Innovation RealTide Project, grant number 727689, and by the Region Hauts-de-France, France in the framework of the project CPER 2015–2020 MARCO. The authors would like to gratefully acknowledge Benoît Gaurier and Maria Ihennicheu involved in the experimental database generation and to warmly thank Thomas Baccetti and Jean-Valery Facq for their assistance and precious advices.

References

- Adcock, T., Draper, S., Willden, R., Vogel, C., 2020. The fluid mechanics of tidal stream energy conversion. *Annu. Rev. Fluid Mech.* 53, 287–310.
- Adrian, R.J., Moin, P., 1988. Stochastic estimation of organized turbulent structure: Homogeneous shear flow. *J. Fluid Mech.* 190, 531–559.
- Ahmadi, M., Yang, Z., 2021. On wind turbine power fluctuations induced by large-scale motions. *Appl. Energy* 293, 1–11.
- Allmark, M., Ellis, R., Lloyd, C., Ordóñez-Sánchez, S., Johansen, K., Byrne, C., Johnstone, C., O'Doherty, T., Mason-Jones, A., 2020. The development, design and characterisation of a scale model horizontal axis tidal turbine for dynamic load quantification. *Renew. Energy* <http://dx.doi.org/10.1016/j.renene.2020.04.060>.
- Bandi, M.M., 2017. Spectrum of wind power fluctuations. *Phys. Rev. Lett.* 118, 1–5. <http://dx.doi.org/10.1103/PhysRevLett.118.028301>.
- Blackmore, T., Myers, L.E., Bahaj, A.S., 2016. Effects of turbulence on tidal turbines: Implications to performance, blade loads, and condition monitoring. *Int. J. Mar. Energy* 14, 1–26. <http://dx.doi.org/10.1016/j.ijome.2016.04.017>.
- Bonnet, J., Cole, D., Delville, J., Gläuser, M., Ukeiley, L., 1994. Stochastic estimation and proper orthogonal decomposition : Complementary techniques for identifying structure. *Exp. Fluids* 17, 307–314.
- Bossuyt, J., Meneveau, C., Meyers, J., 2017. Wind farm power fluctuations and spatial sampling of turbulent boundary layers. *J. Fluid Mech.* 823, 329–344. <http://dx.doi.org/10.1017/jfm.2017.328>.
- Chamorro, L.P., Hill, C., Neary, V.S., Gunawan, B., Arndt, R.E.A., Sotiropoulos, F., 2015. Effects of energetic coherent motions on the power and wake of an axial-flow turbine. *Phys. Fluids* 27. <http://dx.doi.org/10.1063/1.4921264>.
- Druault, P., Delville, J., Bonnet, J., 2005. Experimental 3d analysis of the large scale behaviour of a plane turbulent mixing layer. *Flow Turbul. Comb.* 74, 207–233.
- Druault, P., Gaurier, B., Germain, G., 2022. Spatial integration effect on velocity spectrum: Towards an interpretation of the $-11/3$ power law observed in the spectra of turbine outputs. *Renew. Energy* 181, 1062–1080.
- Druault, P., Gloerfelt, X., Mervant, T., 2011. Investigation of flow structures involved in sound generation by two- and three-dimensional cavity flows. *Comput. & Fluids* 48, 54–67.
- Druault, P., Yu, M., Sagaut, P., 2010. Quadratic stochastic estimation of far field acoustic pressure with coherent structure events in a 2D compressible plane mixing layer. *Internat. J. Numer. Methods Fluids* 62, 906–926.
- Durán Medina, F.G., Calif, R., Germain, G., Gaurier, B., 2017. Turbulence analysis and multiscale correlations between synchronized flow velocity and marine turbine power production. *Renew. Energy* 112, 314–327. <http://dx.doi.org/10.1016/j.renene.2017.05.024>.
- Durgesh, V., Naughton, J., 2010. Multi-time-delay lse-pod complementary approach applied to unsteady high-reynolds-number near wake flow. *Exp. Fluids* 49, 571–583.
- Ebdon, T., Allmark, M.J., O'Doherty, D.M., Mason-Jones, A., O'Doherty, T., Germain, G., Gaurier, B., 2020. The impact of turbulence and turbine operating condition on the wakes of tidal turbines. *Renew. Energy* <http://dx.doi.org/10.1016/j.renene.2020.11.065>.
- Gao, L., Yang, S., Abraham, A., Hong, J., 2020. Effects of inflow turbulence on structural response of wind turbine blades. *J. Wind Eng. Ind. Aerodyn.* 199.
- Gaurier, B., Druault, P., Ihennicheu, M., Germain, G., 2020a. Experimental analysis of the shear flow effect on tidal turbine blade root force from three-dimensional mean flow reconstruction. *Phil. Trans. R. Soc. A* 378, 1–14. <http://dx.doi.org/10.1098/rsta.2020.0001>.
- Gaurier, B., Germain, G., Facq, J.V., Johnstone, C., Grant, A.D., Day, A.H., Nixon, E., Di Felice, F., Costanzo, M., 2015. Tidal energy round robin tests comparisons between towing tank and circulating tank results. *Int. J. Mar. Energy* 12, 87–109. <http://dx.doi.org/10.1016/j.ijome.2015.05.005>.
- Gaurier, B., Ihennicheu, M., Germain, G., Druault, P., 2020b. Experimental study of bathymetry generated turbulence on tidal turbine behaviour. *Renew. Energy* 156, 1158–1170. <http://dx.doi.org/10.1016/j.renene.2020.04.102>.
- Ihennicheu, M., Germain, G., Druault, P., Gaurier, B., 2019a. Experimental study of coherent flow structures past a wall-mounted square cylinder. *Ocean Eng.* 182, 137–146.
- Ihennicheu, M., Germain, G., Druault, P., Gaurier, B., 2019b. Experimental study of coherent flow structures past a wall-mounted square cylinder. *Ocean Eng.* 182, 137–146.
- Lu, P., Ye, L., Zhao, Y., Dai, B., Pei, M., Tang, Y., 2021. Review of meta-heuristic algorithms for wind power prediction: Methodologies, applications and challenges. *Appl. Energy* 301, 117446.
- Lumley, J., 1967. The structure of inhomogeneous turbulent flows. In: Yaglom, Tatarsky (Ed.), *Atm. Turbul. and Radio Wave Prop.* pp. 166–178.
- Magnier, M., Druault, P., Gaurier, B., Germain, G., 2020. Comparison of bathymetry variation effects on tidal turbine behaviour. In: 17^{es} Journées de l'Hydrodynamique. Cherbourg, France.
- Murray, N., Ukeiley, L., 2007. Modified quadratic stochastic estimation f resonating subsonic cavity flow. *J. Turbul.* 8, 1–23.
- Ouro, P., Stoesser, T., 2019. Impact of environmental turbulence on the performance and loadings of a tidal stream turbine. *Flow Turbul. Combust.* 102, 613–639. <http://dx.doi.org/10.1007/s10494-018-9975-6>.
- Picard, C., Delville, J., 2000. Pressure velocity coupling in a subsonic round jet. *Int. J. Heat Fluid Flow* 21, 359–364.
- Pinson, P., Madsen, H., 2012. Adaptive modelling and forecasting of offshore wind power fluctuations with markov-switching autoregressive models. *J. Forecast.* 31, 281–313.
- Slama, M., Pinon, G., El Hadi, C., Togneri, M., Gaurier, B., Germain, G., Facq, J., Nuno, J., Mansilla, P., Nicolas, E., Marcille, J., Pacheco, A., 2021. Turbine design dependency to turbulence: An experimental study of three scaled tidal turbines. *Ocean Eng.* 234.
- Thiébaut, M., Filipo, J., Maisondieu, C., Damblans, G., Jochum, C., Kilcher, L., Guillou, S., 2020. Characterization of the vertical evolution of the three-dimensional turbulence for fatigue design of tidal turbines. *Phil. Trans. R. Soc. A* 378.